Thermo-economic study of hybrid parabolic dish solar power plants in different regions of Spain

Irene Heras[a], Judit García-Ferrero[b], Maria Jesús Santos[c], Rosa-Pilar Merchán[d], Alejandro Medina[e] and Antonio Calvo-Hernández[f]

[a] University of Salamanca, Dpt. of Applied Physics, Salamanca, Spain, iheras@usal.es (CA)
[b] jgferrero@usal.es ,[c] smjesus@usal.es ,[d] rpmerchan@usal.es ,[e] amd385@usal.es ,[f] anca@usal.es

Abstract:

Small-scale hybrid parabolic dish Concentrated Solar Power (CSP) systems coupled to a micro-gas turbine are a promising option to obtain electrical energy in a distributed manner. During the day, solar energy is used to produce electricity and the absence of sunlight can be overcome with the combustion of a fossil or renewable fuel. This study presents the technical feasibility and thermo-economic model of a hybridized power plant in different regions of Spain, considering the local climatic conditions.

The implemented model aims to provide a realistic view of the behaviour of the system, using a reduced number of selected parameters with a clear physical meaning. The irreversibilities taking place in all subsystems (solar part, combustion chamber, micro-gas turbine, and the corresponding heat exchangers) have been considered in the model, developed in Mathematica® language. The model considers the instant solar irradiance and ambient temperature dynamically, providing an estimation of the power output, the associated fuel consumption, and the most relevant pollutant emissions (CO_2, CH_4 and NO_2) linked to combustion, for hybrid and combustion only operating modes at selected geographical locations in Spain. The considered power output ranges between 7 to 30 kWe which is achieved by varying the design specifications. The levelized cost of electricity (LCoE) indicator is estimated as a function of investment, interest rate, maintenance and fuel consumption actual costs in Spain. The electricity costs from hybrid parabolic dish are between 22% and 27% lower compared to pure combustion power plant, while specific fuel consumption and therefore CO_2 emissions can be reduced up to 33%. This model shows the potential of hybrid solar dishes to become cost-competitive against non-renewable ones from the point of view of electricity costs and significant reduction in gas emission levels in regions with high solar radiation and low water resources.

Keywords:

Brayton cycle, Distributed generation, Micro gas turbine, Solar parabolic dish, Thermo-economic model.

1. Introduction

Thermosolar power generation has been established as one of the more viable sources of renewable energy [1]. In the last few years it has emerged as a potential solution to supply dispatchable electricity, since it can rely on hybridization or thermal energy storage [2]. The hybridization of a

solar thermal power system with combustion provides a continuous supply of electricity throughout the year, with a much lower investment and maintenance costs than thermal storage [3].

Besides the full dispatchability, hybrid solar thermosolar plants using a Brayton thermodynamic power cycle, present a wide number of advantages over other Concentrated Solar Power (CSP) systems, including the scalability and adaptability to the requirements of the location, higher global efficiencies and low to zero water consumption. The higher exhaust temperature also enables the possibility of include additional services such as thermal energy supply, cooling or water purification [4]. The first generation of hybrid solar gas-turbine power plants were based on existing industrial gas-turbine units [5]. Some test plants EU-funded have demonstrated the Brayton hybrid concept, from small-scale gas-turbines up to 250 kW_e (SOLGATE [6] and SOLHYCO [7]) to scaled up systems such as the full operable prototype SOLUGAS project [8] with its proven combustion chamber and 4.6 MW_e gas turbine. All these hybrid systems were made up of the solar components and a combustion chamber separately.

Conversely, Hybrid Solar Receiver Combustors (HSRC) are a promising technology that integrates into a single device the functions of a solar receiver and a combustor [9]. It has been demonstrated how this machinery reduces the overall costs and net fuel consumption relative to equivalent hybrid solar gas systems [10]. The first-of-a-kind successful demonstration of a HSRC was designed by Chinnici *et al.* [9] employing an annular solar cavity receiver with a combustor at laboratory-scale.

In parallel, the EU-funded OMSoP project developed a CSP plant based on parabolic dish technology that integrates in the volumetric receiver a combustion chamber, joined to a micro-gas turbine (mGT), obtaining a nominal electrical power output of 5 kW_e and air outlet temperatures up to 820°C [11]. This small-scale hybrid CSP plants shows a clear tendency to be attractive for off-grid applications in the distributed energy generation [12] and nowadays can compete against the non-renewable diesel generators or the photovoltaic technology.

The first aim of this study is to extend the dynamic thermodynamic model of a hybrid parabolic dish plant developed previously [13] for the annual evaluation in different locations. Next aim is to estimate the equipments, manufacture, installation and other costs of the system and provide a comprehensive annual appraisal. In order to be able to compare different power plants or operation modes, the minimum electricity sale price or Levelised Cost of Electricity (LCOE), the average solar share and the specific CO_2 emissions have been calculated.

The presented thermodynamic model consists of a paraboloid dish collector and a hybrid solar receiver combustor integrated with a small scale (7 to 30 kW_e) micro-gas turbine located at the focal point of the dish. The algorithm developed under Mathematica® software takes into consideration daily real environmental conditions (temperature and solar radiation) of the chosen locations and a reduced number of parameters of the designed power plant. Precise estimations of the hybrid plant performance have been then calculated (*i.e.* net output power, global efficiency, fuel consumption, solar share, etc, …) for time-dependent conditions and integrated over a year. The hybrid system working mode has been compared against pure combustion operation in three selected locations (Salamanca, Santander and Sevilla) of Spain. This joint thermodynamic and economic assessment could help to identify the optimum design parameters and the operation mode, that yields the minimum specific cost for a selected location.

2. Hybrid parabolic dish micro gas turbine model

In this section is first described the plant configuration and the thermodynamic model employed to simulate the overall plant. The different performance indicators employed for comparing different locations and plant configurations are explained below.

The designed hybrid CSP plant includes a parabolic dish that collects the sun radiation and heats a working fluid (air) flowing in the hybrid receiver situated at the focal point. According to the amount of solar irradiation G and ambient temperature T_L, the integrated combustion chamber could release an energy flow in order to increase the fluid temperature up to a pre-fixed temperature. The inlet turbine temperature is prefixed T_3 so that the power output of the plant is also constant along the day,

regardless the meteorological conditions. As schematized in Fig. 1, the HSRC includes a volumetric solar receiver, a combustion chamber and a mGT operating on a recuperative Brayton cycle. As outlined below, solar part, combustion chamber and power unit main subsystems have been identified for the mathematical model developed.

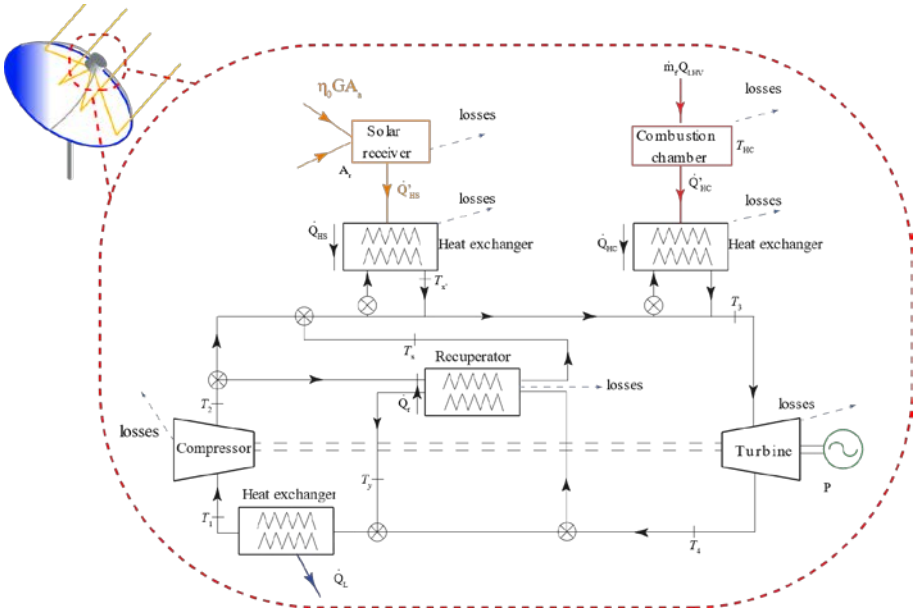

Figure 1. Schematic representation of the hybrid CSP plant composed of the parabolic dish collector and the Hybrid Solar Receiver Combustor which includes the solar receiver, the combustion chamber and the micro gas turbine.

2.1. Thermodynamic model

The mathematical model is based on previous works of our group [14,15]. Main irreversibilities sources are included in the model, such as the losses in the heat exchangers, the non-ideal collector and receiver with its associated radiative, convective and conductive losses, or non-ideal turbine, compressor and recuperator. The integrated mGT with the pressurized closed volumetric receiver is modelled as a single step recuperative Brayton cycle, as represented in the *T*-*S* diagram of Fig. 2 (a). The air inside the closed cycle at ambient temperature T_{amb} is initially compressed. Then is heated up through first, a recuperator by using the high temperature of the gas after the mGT (T_x), and afterwards, by the solar receiver up to $T_{x'}$. In case this heat input does not reach the prefixed turbine inlet temperature T_3, the fluid receives an extra energy input from the combustion chamber. Subsequently, the fluid is expanded at the turbine where the temperature decreases to T_4 and the heat is converted into mechanical work. The mGT generates a high frequency AC output that has to be converted into grid frequency (*i.e.* 50-60 Hz) through an inverter. In the global conversion efficiency, the generator, control system and ratio between shaft power and mGT rotor power (organic efficiency) are considered.

The aperture area A_a of the collector dish and its optical efficiency η_o affects the amounts of solar thermal energy deliver to the receiver $\eta_o G A_a$. The effective heat flow transferred from the solar plant to the working fluid is $\dot{Q}_{HS}$. It is calculated by subtracting from the total thermal energy absorbed by the receiver with solar absorptance α, the radiation, conduction and convection losses that take place in the different components of the receiver.

$$\dot{Q}_{HS} = \varepsilon_{HS}\{\eta_o G A_a \alpha - A_r[\varepsilon\sigma(T_{HS}^4 - T_{amb}^4) + \overline{U_L}(T_{HS} - T_{amb})]\} \quad (1)$$

where ε_{HS} is the solar heat exchange efficiency, ε is the receiver emittance, $\overline{U_L}$ is the conduction-convection heat transfer coefficient and T_{HS} is the working temperature of the solar collector.

The solar energy contribution can also be expressed by the fluid temperature change from the regenerator output T_x up to the combustion chamber. The working fluid is considered as ideal gas with mean value of specific heat c_w. Regarding the combustion chamber, the transferred heat flow ($\dot{Q}_{HC} = \varepsilon_{HC}\, \eta_c\, \dot{m}_f\, Q_{LHC}$) depends its heat exchange efficiency ε_{HC}, the chamber efficiency η_c, the fuel mass flow rate $\dot{m}_f$ and the low heating value Q_{LHC} of the fuel type employed. Natural gas is considered in this study, but it may be replaced by renewable fuels such as biogas. The overall energy transfer flow of the hybrid plant upwards the micro gas turbine is schematized in Fig. 2 (b).

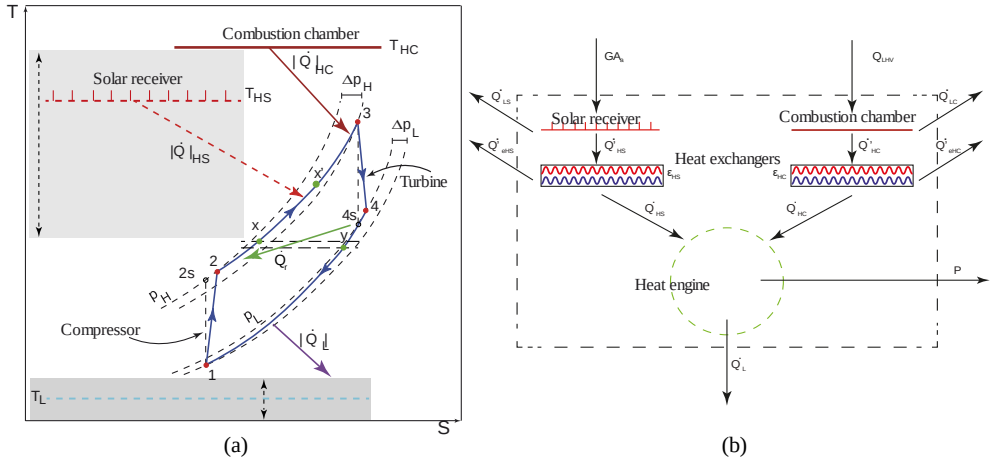

Figure 2. (a) Schematic T-S diagram and (b) energy transfer diagram of the modelled recuperative Brayton cycle.

An often-overlooked issue is the need for high-temperature and high-pressure in the hybrid receiver combustor. The maximum tolerated air temperature in the HSRC is determined chiefly by the resistance of the materials of the different components (i.e. receiver materials, turbine blades, …). A monitoring system based in the meteorological forecast and instant climatic conditions should be installed to deviate collector from direct beam radiation when the limit temperature, delimited by the thermal resistance of the components [16], can be exceeded to prevent serious deterioration.

2.2. Performance indicators

The performance of the plant can be quantified through applying appropriate indicators. In order to consider the different aspects of the power generation system, a combination of thermodynamic, environmental and thermo-economic indicators were employed in this paper.

2.1.1. Thermodynamic performance indicators

The overall thermal efficiency η is the ratio between the delivered net power and the total heat input, as defined in (2).

$$\eta = \frac{P}{GA_a + \dot{m}_f Q_{LHV}} = \eta_h \eta_s \eta_c \left(\frac{\varepsilon_{HS}\varepsilon_{HC}}{\eta_c f \varepsilon_{HC} + \eta_s (1-f)\varepsilon_{HS}} \right) \tag{2}$$

It can also be expressed in an analytical way in terms of the efficiencies of each subsystem (solar part η_s, combustion chamber η_c and gas turbine η_h, defined in (3)), the heat exchangers (ε_{HS} and ε_{HC}) that connect them and the solar share f.

$$\eta_s = \frac{|\dot{Q}'_{HS}|}{GA_a};\ \eta_C = \frac{|\dot{Q}'_{HC}|}{\dot{m}_f \cdot Q_{LHV}};\ \eta_h = \frac{P}{|\dot{Q}_{total}|} = \frac{P}{|\dot{Q}_{HS}| + |\dot{Q}_{HC}|} \tag{3}$$

The solar share f is the ratio between the available solar input and the total heat absorbed by the working fluid. This indicator relates the degree of solar irradiation used in the hybrid solar plants or

the share of the electricity that has actually been generated from the solar energy. When there is a pure solar operation mode, solar share equals to one and it becomes null when there is no solar contribution, as during the night or cloudy days.

The mass flow fuel consumption $\dot{m}_f$ is derived from the heat input coming from the combustion chamber. Hereof, the specific greenhouse gas emissions arising from the fuel amount over a period of time are estimated from the amount and type of fuel employed. In particular, daily and annual emissions of CO_2, N_2O and CH_4 gases were evaluated as being the main ones associated with the combustion of natural gas.

2.2.3 Economic performance indicators

Nowadays, it is necessary to evaluate not only the technical aspects of a power plant, but also to assign costs and to identify the intensity of harmful emissions. Therefore, once the thermodynamic performance of the plant is established, the second stage is to assign costs to the power plant of both initial installation costs CI_0 and costs incurred during operation: indirect and maintenance costs $C_{O\&M}$, such as labour to operate the plant or water for cleaning the mirrors. The levelized Cost of Electricity (LCoE) is an economic indicator commonly employed to compare power plants with different sizes and it serves to determine the minimum electricity sale price needed to recover investments costs over the expected lifetime of the plant. Equation (4), describes the *LCoE* calculation following the International Energy Agency (IEA) definition [17]. It includes the sum of the total cost to the sum of the electrical energy production over the expected lifetime *n*, which is assumed to be 25 years for solar plants. Both dividends are discounted at a constant rate *r* over the lifetime of the plant. Additionally, in the case of hybrid plants, the fuel cost C_{fuel} has to be included.

$$LCoE = \frac{\sum_{i=1}^{n}\left(CI_0 + C_{O\&M_i} + C_{fuel_i}\right)(1+r)^{-i}}{\sum_{i=1}^{n} E_i(1+r)^{-i}} \tag{4}$$

Neither the decommissioning costs nor the interest accrued during the construction are considered, as the construction time for these parabolic dishes is considered lower than 1 year. In this paper, the total investment costs are expressed in (5), derived from the sum of the equipment cost C_{eqp}, the cost of equipment installation C_{inst}, civil engineering costs C_{civil} and contingencies C_{cont}.

$$CI_0 = \sum C_{eqp} + C_{inst} + C_{civil} + C_{cont};\ \sum C_{eqp} = C_{HSRC} + C_{dish} + C_{gen} \tag{5}$$

The main constituents of the CSP plant are identified to evaluate the overall purchase equipment cost, which is equal to the summation of each single element: the hybrid solar receiver-combustor (gas turbine-expander, compressor, auxiliary parts such as insulation or housings and combustion chamber), solar receiver (control system, absorber, pressurized resistant glass window), dish collector (tracking system, mirror facets, pedestal) and the electrical generator (power electronics and control system), as expressed in (5). The combustion chamber costs, with its corresponding fuel pump and control system costs, are included together within the mGT cost function.

3. Data description and validation

The aforementioned publications of the group [13–15], have already validated the thermodynamic model employed here for static design point conditions by comparing with the results presented by Semprini *et al.* [18]. Based in the accurate fitting of the overall results between both models, a dynamic study is carried out here for an extended period of time: one year. As detailed below, the model is implemented for two output powers in three different locations of Spain.

3.1. Data employed for the model

The main characteristics of each component of the system are summarized in Table 1, together with the assumptions and losses parameters implemented for the two power outputs considered: 30 and 7

kW_e. Pressurized air is selected as heat transfer fluid, considering as ideal gas. The mean values of pressure specific heat $\bar{c}_w$ and adiabatic coefficient $\bar{\gamma}$ are calculated from a temperature varying specific heat $c_w(T)$ fourth order polynomial. The coefficients of the fits were taken from [19] at an average pressure of p =1.9 bar. An adjustment of the air mass flow rate $\dot{m}$ and the pressure ratio r_p for each power output enables to obtain the target power values for prefixed system limitations (turbine inlet temperature T_3 = 1170K).

Table 1. Parameters employed for the hybrid calculation of 30 and 7 kW_e output power.

Parameter		*30 kWe*	*7 kWe*	Unit
Optical efficiency of the parabolic dish	η_0	0.941	0.946	
Aperture area of the parabolic dish	A_a	211.80	52.80	m^2
Area of the solar receiver window	A_r	0.1182	0.0296	m^2
Solar absorptance	α	0.96	0.96	
Thermal emittance	ε	0.10	0.10	
Solar heat exchange efficiency	ε_{HS}	0.795	0.792	
Turbine isentropic efficiency	ε_t	0.76	0.74	
Compressor isentropic efficiency	ε_c	0.77	0.76	
Recuperator efficiency	ε_r	0.85	0.85	
Pressure ratio	r_p	3.84	3.65	
Mass flow rate	$\dot{m}$	0.3379	0.0881	kg/s

The efficiencies of the solar and power cycle components are indicated in the table, based on the work by Semprini *et al.* work [18]. The pressure drops irreversibilities factors associated to the heat input (ρ_h) and heat release (ρ_l) are set to 0.98 and 1, respectively. The combustion chamber integrated into the HSRC has an efficiency of η_c and heat exchange efficiency ε_{HS} equals to 0.97 in both cases. Natural gas is employed as fuel in the combustion chamber, which has a lower heating value Q_{LHC} of 47.141 MJ/kg.

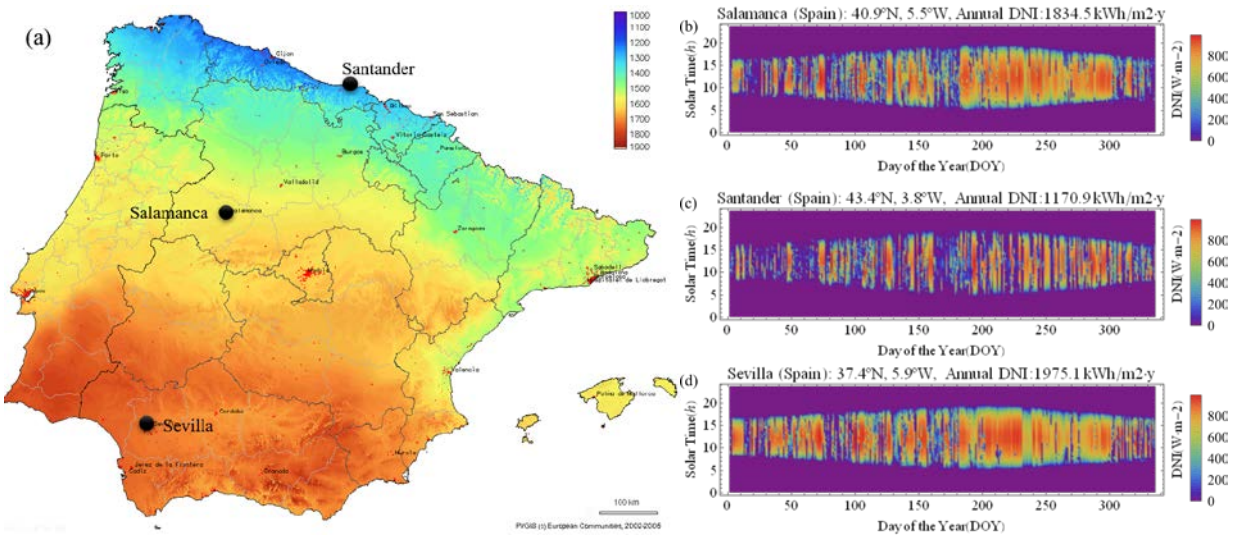

Figure 3. (a) Distributed map of the yearly total global horizontal irradiation (kWh/m^2) in Spain and Portugal [20]. *Annual DNI map from December of 2017 until November of 2018 in (b) Salamanca, (c) Santander and (d) Sevilla. The annual DNI accumulated during this period is indicated above each figure of each city.*

The annual performance of the plant is estimated in three locations of Spain as pointed in Fig 3 (a). Last year ambient temperature T_{amd} and Direct Normal Irradiation G real data were provided by the Spanish meteorological national agency (AEMET) and averaged every 30 minutes, for the three selected emplacements. Figures 3 (b), (c) and (d) show the radiation map of Salamanca, Santander and Sevilla, respectively, giving the solar irradiation intensity in function of the time of the day and day of the year. Between these locations, Sevilla has the largest annual DNI accumulated (1971.5

kWh·m^{-2}), meanwhile Santander (with annual DNI accumulated of 1170.9 kWh·m^{-2}) shows a great variability in the solar resource due to its frequent cloudy days. Regarding the annual temperatures (not represented here), there is also a huge difference between locations and on average it from 5 to 15ºC hotter in Sevilla than in Salamanca along the year.

The temperature attained at the solar receiver (T_{HS}) has been dynamically calculated for every pair of values T_{amb} and G of one day per month, by equalling the heat rate released by the receiver and the heat input absorbed. Then, yearly performances of the plant are averaged considering the number of days per month. The daily averages of the solar dependent indicators (T_{HS}, f and η_s) are calculated only during the effective insolation hours (G > 15 Wm^{-2}). The generated mechanical power output (P) of the mGT has to be converted into electric energy by the electrical generator. The final electrical power output E_{elec} of the generator is computed after subtracting the electrical and mechanical efficiencies (η_{elec}= 0.94; η_{mec} = 0.98) from the net mGT power: $E_{elec} = \eta_{elec} \cdot \eta_{mec} \cdot P$. Then, the net electrical power output is integrated through the year to obtain the annual generated energy.

3.2. Economic data employed

Assembling a wide variety of sources including literature sources and direct personal communications, specific cost functions have been determined to calculate the final purchasing costs of each element, based on the size and operation conditions. This hybrid solar power plant within its specific HSRC is still not currently marketed, however, to draw price comparisons, a prototype of integrated combustion chamber and mGT based on Ragnolo *et al*. [21] is employed. Many factors will affect the final purchasing costs such as the number of units ordered or the state of the market. Therefore, the data provided here is useful for comparison between locations and operations modes, but it could not be deemed as exact costs predictions of a hybrid solar power plant. The purchased equipment costs are estimated assuming a production rate of 2000 modules year, as described in [22].

Following recommendations from Peters and Timmerhaus [23], the cost of equipment installation C_{inst} is equal to 20% of the initial equipment purchasing costs. Likewise, civil cost C_{inst}, including project engineering costs, is calculated by 8 to 23 % of the total C_{eqp}. The unforeseen regulatory of technical problems during the construction or operations, the IEA estimates a total contingency cost C_{cont} equal the 10% of the total initial investment cost. Contrary to initial investment costs, operation and maintenance costs $C_{O\&M}$ are incurred during the power plant lifetime such as water consumption for occasional mirror facets cleaning (50 l/m^2 per year) and costs related to reparation or replacement of damaged components, calculated as a percentage of the initial equipment cost (*i.e.* 2%/yr for the mGT and receiver, 3% /yr for the elements of the parabolic dish, and 4%/yr for the control system). Due to the small plant size, no specific operation labour costs are considered, and the technician or operator is included within the maintenance costs detailed above.

4. Results

The evaluation of the performance of solar power plants or other renewable energy systems is complicated by the fact that operation of the plant is strongly dependant on the local meteorological conditions, which can vary significantly throughout the day and the year. In order to determine the power output, efficiencies of the subsystems, fuel consumptions and greenhouse gas emissions over the year, dynamic calculations are performed from the real data for the three locations. In this section it is first compared one day performance of the three locations and subsequently the annual analysis of both hybrid and pure combustion operating modes. Finally, combining the results of the dynamic evaluation with the subsystem cost functions, a thermoeconomic analysis for the considered locations is developed and the results are analysed and compared.

4.1. Daily variations performance

To enable a daily comparative assessment, an Autumn day (October 13th, 2018) is selected to explain the differences in the thermodynamic behaviour of a 30 kW$_e$ hybrid power plant emplaced in the three selected locations. The daily T_{amb} changes are quite similar among the locations, however, great

differences are observed in G, displaying maximum values of 600 and 460 and 820 $W \cdot m^{-2}$ during the central hours in Salamanca, Santander and Sevilla, respectively, with a peak of 840 at 15h in Salamanca.

In Fig. 4, the values of the efficiencies (η_s, η_h and η) and the solar share are plotted against day time. The conversion of solar radiation into heat (or solar efficiency η_s) shows no wide divergencies between the cities and it remains almost unchanged $\eta_s \approx 0.89$ along the sunshine hours. This value depends mainly on the temperature reached in the receiver and on the configuration of the solar subsystem, similar in all cases. The efficiency of the power block does not vary through the day and it has an almost constant value $\eta_h \approx 0.24$ to 0.26, which guarantees a power output constant independent of the fluctuations in the solar radiation. Regarding the overall efficiency of the plant does not vary during the night without solar contribution ($\eta \approx 0.252$), and it decreases when solar subsystem comes into play, as neither optical losses nor radiation or convection losses affect to the plant. The solar share f is depicted during the effective insolation hours, showing values below 0.7 in both Salamanca and Santander meaning that the combustion chamber is required to achieve the fixed inlet temperature of the turbine. On the other hand, in Sevilla from 9 to 15 h the solar share reaches f=1, implying the plant operates in pure solar mode without requiring fuel combustion.

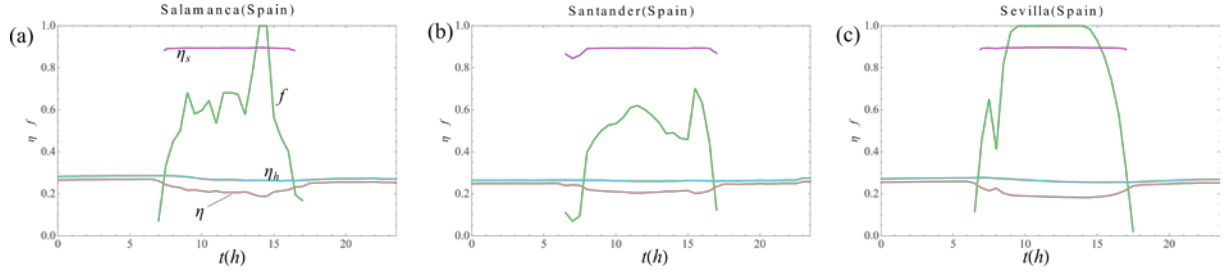

Figure 4. Daily variation of solar share f, solar efficiency η_s, Brayton cycle efficiency η_h and overall efficiency η in a 30 kWe power plant in (a) Salamanca, (b) Santander and (c) Sevilla for October 13th, 2018 against time in UTC hours. f and η_s are only represented for effective insolation hours.

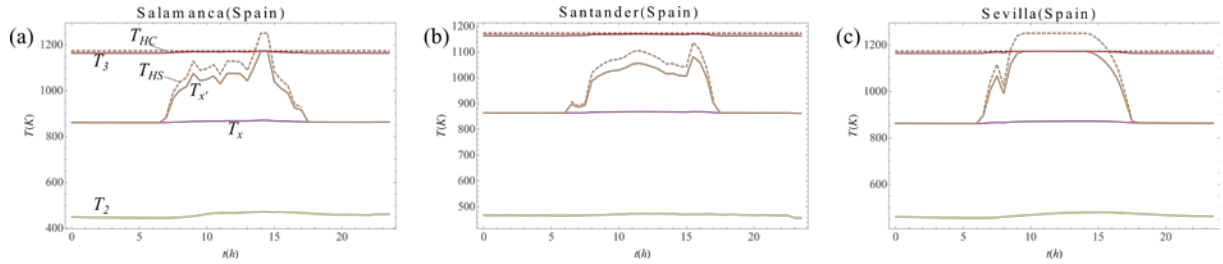

Figure 5. Daily variation of the Brayton cycle temperatures in a 30 kWe power plant in (a) Salamanca, (b) Santander and (c) Sevilla for October 13th, 2018 against time in UTC hours.

The daily variations of temperatures are plotted in Fig. 5. As might be expected from previous figure, the temperature achieved in Sevilla from the solar subsystem ($T_{x'}$) equals the turbine inlet temperature in the central hours of the day. This wide plateau during the higher insolation hours is due to the fact that the maximum temperature is limited up to 1173 K (by *i.e.* by a defocusing system) to avoid damaging the plant components. In the other two locations, the temperatures vary according to T_{amb} and G. The compressor outlet temperature and the temperature after the recuperator are nearly constant with values of $T_2 \approx 450$ K and $T_x \approx 850$ K, respectively, and they oscillate following T_{amb}. The temperature after the turbine expansion (not represented here) is independent on the location and day and has a value of $T_4 \approx 930$ K. This high temperature is harnessed through the recuperator to increase the temperature after the compression step, but it could be additionally employed for cogeneration and thermal energy production.

The variation of the heat input along the day is plotted in Fig. 6, where is distinguished heat coming from the solar (Q_{HS}) and combustion chamber (Q_{HC}) subsystems. The total input heat ($Q_{total} = Q_{HS} + Q_{HC}$) is roughly constant along the day, whereas both Q_{HS} and Q_{HC} oscillates according to the solar

resource. Overnight all the heat proceeds from the fuel combustion while during the day there is a combination according to the impugning solar radiation into the parabolic dish.

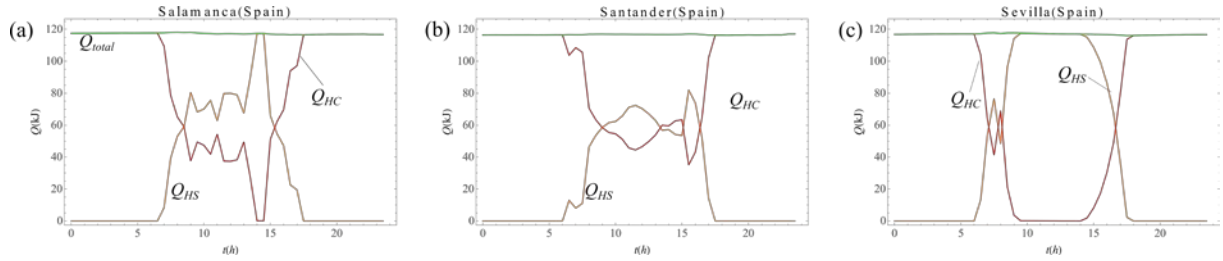

Figure 6. Daily solar heat Q_{HS}, combustion chamber heat Q_{HC} and total input heat Q_{total} in a 30 kWe power plant in (a) Salamanca, (b) Santander and (c) Sevilla for October 13th, 2018 against time in UTC hours.

4.2 Annual performance

The yearly averages of overall plant efficiency and solar share, as well as the annual accumulated fuel consumption, gas emissions and generated energy are summarized in Table 2 for two power outputs (30 and 7 kW_e). For the sake of completeness, a pure combustion mode is also calculated in which similar output power is obtained by using only the combustion chamber to heat the working fluid.

Table 2. Summary of the annual results for different locations for hybrid and pure combustion modes.

Location	Salamanca		Santander		Sevilla	
Power output	*30 kW_e*	*7 kW_e*	*30 kW_e*	*7 kW_e*	*30 kW_e*	*7 kW_e*
Hybrid operation mode						
Global efficiency (%)	24.89	23.15	25.04	23.36	23.84	22.11
Averaged solar share	0.32	0.30	0.21	0.22	0.43	0.41
Energy generated (MWh)	262.98	61.41	259.18	60.46	256.37	59.73
Fuel consumption (t)	61.31	15.44	69.55	17.37	54.59	13.76
Combustion operation mode						
Energy generated (MWh)	271.50	63.56	263.72	61.59	264.54	61.80
Fuel consumption (t)	82.11	20.63	81.80	20.56	81.83	20.55
Mode comparison						
Fuel savings (t)	20.79	5.19	12.25	3.19	27.24	6.80
(Fuel savings (%))	(25.3%)	(25.2%)	(15.0%)	(15.5%)	(33.3%)	(33.0%)
Reduction of CO_2 (t)	51.45	12.84	30.23	7.89	67.41	16.82
Reduction of CH_4 (kg)	973.56	242.99	573.68	149.27	1275.37	318.29
Reduction of N_2O (kg)	95.52	23.59	55.70	14.49	123.82	30.90
Economic indicators						
LCoE (€/MWh)	125.37	131.65	137.51	144.74	119.55	125.65

The differences between hybrid and pure combustion modes are expressed in terms of energy generated and fuel consumption. The integrated energy over a year differs in a 3%, lower in the hybrid mode due the losses incurred the collector and solar receiver. Comparing between locations, the generated energy is slightly higher in Salamanca, even than in Sevilla with higher solar radiation. This is justified by the fact that the final power output depends only in the ambient temperature, and for lower temperatures, the Brayton cycle efficiencies are higher. The monthly distribution of the overall efficiencies is represented in Fig. 7 (a) for a power plant of 30 kW_e. Sevilla shows the lower efficiency along the year and the minimum values are observed in the summer months when *f* is higher. The annual averages are around 25.04 %, 24.86% and 23.84 for Santander, Salamanca and Sevilla, respectively.

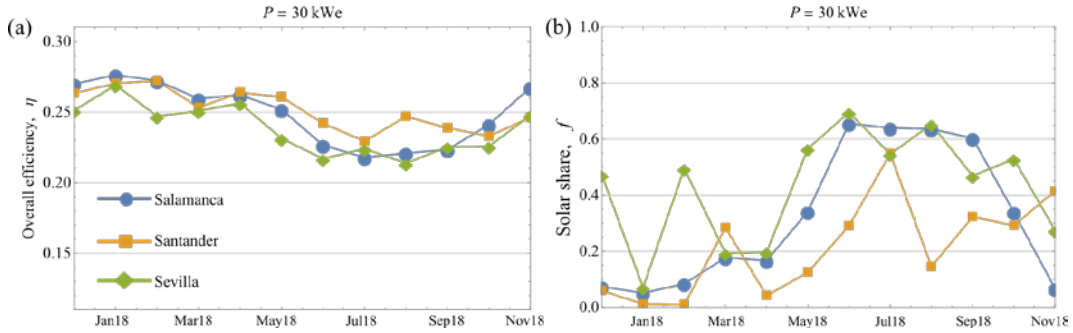

Figure 7. Monthly distribution performances of the hybrid parabolic dish of 30kWe (a) Overall efficiency and (b) solar share

Figure 7 (b) shows the monthly distribution of the solar share, averaged only during the effective insolation hours ($G > 15\ W \cdot m^{-2}$). This value varies from the hottest months, achieving average values of $f \approx 0.7$ in Sevilla, to winter in Santander, where $f \approx 0$, city characterised by abundant cloud cover and frequent precipitations.

The monthly differences in fuel consumed are plotted in Fig. 8 for both hybrid and pure combustion modes. In terms of fuel consumption, all the electricity comes from the combustion of natural gas overnight and in the combustion mode. It is noticeable that the fuel savings depends on the location and month, saving up to 33.3%, 27.2 t (6.8 t) of natural gas in Sevilla for a hybrid parabolic dish of 30 kW_e (7 kW_e). Hence, this implies a further saving of ≈12000€/year in natural gas in Sevilla, ≈9200€ in Salamanca and ≈5400€ in Santander per year due if the hybrid configuration is employed.

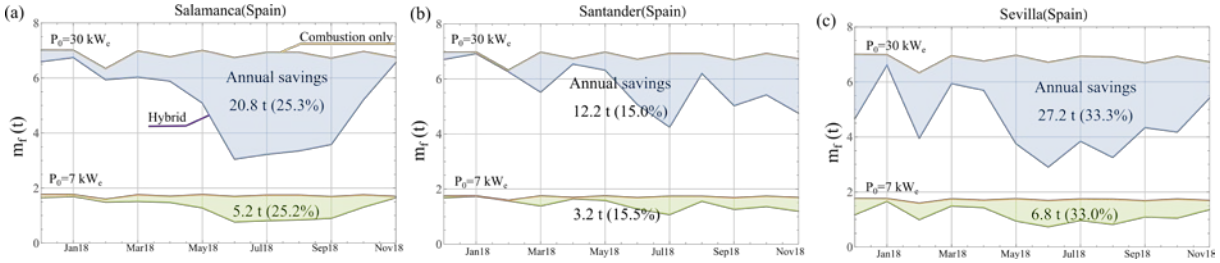

Figure 8. Monthly distribution fuel consumption for a power plant of 30 and 7kWe in both hybrid and combustion only operation modes of (a) Salamanca, (b) Santander and (c) Sevilla. The total fuel saved along the year is indicated in the figure for the two output powers.

The main greenhouse gas emissions (CO_2, CH_4 and NO_2) have been derived from the total fuel consumption. In the case of a hybrid plant of 30kW_e emplaced in Sevilla, there is a considerable reduction associated of 67.4 t of CO_2, 1275.4 kg of CH_4 and 123.8kg of NO_2.

4.3. Economical results

The thermo-economic indicator is studied in this section to compare between the three different locations and power levels. The economic performance of the 30 and 7 kW_e power plants are represented in Figs. 8 (a) and (b), respectively, in terms of the gas natural price, based on IEA and ECOSTAR figures for Europe. The prices vary significantly between locations and time, and at the time of writing, it is assumed to be 7.72 €/MMbtu in Europe. As can be seen in Fig. 8 and in Table 2, Sevilla, with the highest solar irradiation, presents the lower LCoE for both plant dimensions and fuel prices, with 119.5 €/MWh, compared to 137.51 €/MWh in Santander the for the same 30 kW_e hybrid plant. In the case of Salamanca (with a 7% lower solar radiation than Sevilla), the prices are only a 4% higher than the ones in Sevilla, obtaining 125.37 €/MWh for the 30 kW_e power plant and 131.65 €/MWh for the 30 kW_e one.

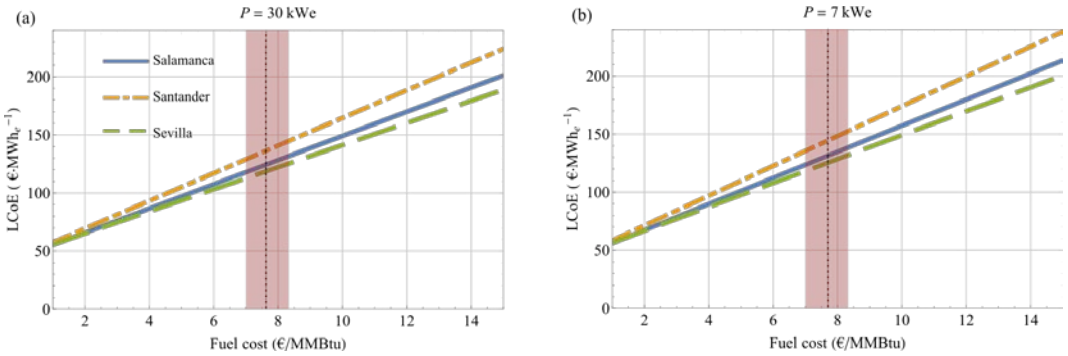

Figure 9. Levelised cost of energy in Salamanca, Santander and Sevilla against natural gas cost for a hybrid paralic dish with averaged output power of (a) 30 kW_e and (b) 7kW_e. The fuel range price in Europe and selected price are indicated in the figures.

5. Conclusions and outlook

A thermodynamic model has been developed in Mathematica® for a parabolic dish CSP plant consisting on a hybrid solar receiver combustor with a Brayton micro gas turbine and a pressurized volumetric receiver. The system, already validated, is described with a reduced number of parameters. A dynamic study is carried out in three Spanish locations (Salamanca, Santander and Sevilla) by employing real T_{amb} and G values as function of day time for two different power outputs: 30 and 7 kW_e. These systems are ideally suited for off-grid applications, as they deliver an approximately constant output power independently on the meteorological conditions and emplacement chosen. The high concentration ratio attainable by a parabolic dish allow reaching high temperatures, with a consequent cycle efficiency increase, achieving annual averages up to 25%. However, the combination of high temperature and high gas fluxes makes the HSCR a critical component of the system, and innovative designs are needed to ensure efficient and reliable operation.

Annual performance simulations are a helpful tool to assess the overall yearly behaviour and costs of the modelled system and compare between hybrid and pure combustion operation modes. The higher annual solar irradiation in Sevilla increases considerable the solar share, working in pure solar mode in the central hours of the days more than half of the year. Accordingly, the fuel consumption and greenhouse gas emissions could be reduced up to 33.3% as compared with a pure combustion plant with similar power output.

Finally, the economic potential of the hybrid parabolic dish power plant is analysed. The precise estimation of the costs of any given piece of the power plant is one of the main challenges in order to accurately determine the economic performance. The final costs depend not only in the size or operating conditions but also on the current state of the market, the pricing policy adopted by the manufacturer or the number of units ordered. All these factors will affect the final purchasing costs. The lowest achieved LCoE values are 119.55 and 125.37 €/MWh, obtained in Sevilla and Salamanca, respectively, for the higher output power plants. The cost of fuel is a major factor when calculating the LCoE, showing a large influence the fuel selection in hybrid solar thermal systems. Further study on renewable biofuels are required in order to search efficient and clean electric energy in a distributed way with lower production costs.

Acknowledgments

Financial support from Junta de Castilla y León of Spain (project SA017P17) and Plan TCUE 2018-2020 “Proof of Concept” are acknowledged. The authors would like to thank AEMET services for the meteorological data provided.

References

[1] Köberle AC, Gernaat DEHJ, van Vuuren DP. Assessing current and future techno-economic potential of concentrated solar power and photovoltaic electricity generation. Energy 2015;89:739–56.

[2] Powell KM, Rashid K, Ellingwood K, Tuttle J, Iverson BD. Hybrid concentrated solar thermal power systems: A review. Renew Sustain Energy Rev 2017;80:215–37.

[3] Giuliano S, Buck R, Eguiguren S. Analysis of Solar-Thermal Power Plants With Thermal Energy Storage and Solar-Hybrid Operation Strategy. J Sol Energy Eng 2011;133:031007.

[4] Aichmayer L, Spelling J, Laumert B, Fransson T. Micro Gas-Turbine Design for Small-Scale Hybrid Solar Power Plants. J Eng Gas Turbines Power 2013;135:113001.

[5] Korzynietz R, Brioso JA, Del Río A, Quero M, Gallas M, Uhlig R, et al. Solugas - Comprehensive analysis of the solar hybrid Brayton plant. Sol Energy 2016;135:578–89.

[6] European Commission. SOLGATE: Solar hybrid gas turbine electric power system. Final Publishable Report. 2005.

[7] Heller P, Denk T. SolHyCo project: (SOLar HYbrid power and COgeneration plants). Final public Report, SES6-CT-2005-019830.

[8] Quero M, Korzynietz R, Ebert M, Jiménez AA, Del Río A, Brioso JA. Solugas - Operation experience of the first solar hybrid gas turbine system at MW scale. Energy Procedia 2013;49:1820–30.

[9] Chinnici A, Nathan GJ, Dally BB. Experimental demonstration of the hybrid solar receiver combustor. Appl Energy 2018;224:426–37.

[10] Nathan GJ, Battye DL, Ashman PJ. Economic evaluation of a novel fuel-saver hybrid combining a solar receiver with a combustor for a solar power tower. Appl Energy 2014;113:1235–43.

[11] Aichmayer L, Spelling J, Laumert B. Preliminary design and analysis of a novel solar receiver for a micro gas-turbine based solar dish system. Sol Energy 2015;114:378–96.

[12] Lim JH, Dally BB, Chinnici A, Nathan GJ. Techno-economic evaluation of modular hybrid concentrating solar power systems. Energy 2017;129:158–70.

[13] Santos MJ, Merchán RP, Medina A, Hernández AC. Micro Gas Turbine and Solar Parabolic Dish for distributed generation. Renew. Energy Power Qual. J., 2018, p. 340.

[14] Olivenza-León D, Medina A, Calvo Hernández A. Thermodynamic modeling of a hybrid solar gas-turbine power plant. Energy Convers Manag 2015;93:435–47.

[15] Santos MJ, Merchán RP, Medina A, Calvo Hernández A. Seasonal thermodynamic prediction of the performance of a hybrid solar gas-turbine power plant. Energy Convers Manag 2016;115:89–102.

[16] Ho CK, Iverson BD. Review of high-temperature central receiver designs for concentrating solar power. Renew Sustain Energy Rev 2014;29:835–46.

[17] Dowling AW, Zheng T, Zavala VM. Economic assessment of concentrated solar power technologies: A review. Renew Sustain Energy Rev 2017;72:1019–32.

[18] Semprini S, Sánchez D, De Pascale A. Performance analysis of a micro gas turbine and solar dish integrated system under different solar-only and hybrid operating conditions. Sol Energy 2016;132:279–93.

[19] Lemmon EW, Huber ML, McLinden MO. NIST Standard Reference Database 23: Reference Fluid Thermodynamic and Transport Properties-REFPROP, Version 9.1 2013.

[20] Geographical Assesment of SolSolar Resource. Institute of Energy and Trasnport (IET) European Comission n.d. http://re.jrc.ec.europa.eu/pvgis/ (accessed February 20, 2019).

[21] Ragnolo G, Aichmayer L, Wang W, Strand T, Laumert B. Technoeconomic Design of a Micro Gas-turbine for a Solar Dish System. Energy Procedia 2015;69:1133–42.

[22] Gavagnin G, Sánchez D, Martínez GS, Rodríguez JM, Muñoz A. Cost analysis of solar thermal power generators based on parabolic dish and micro gas turbine: Manufacturing, transportation and installation. Appl Energy 2017;194:108–22.

[23] Peters MS, Timmerhaus K, West RE. Plant Design and Economics for Chemical Engineers. 5th ed. McGraw-Hill Education; 2002.